Localizing Objects in 3D from Egocentric Videos with Visual Queries

Jinjie Mai Abdullah Hamdi Silvio Giancola Chen Zhao Bernard Ghanem

King Abdullah University of Science and Technology (KAUST)

{jinjie.mai,abdullah.hamdi,silvio.giancola,chen.zhao,bernard.ghanem}@kaust.edu.sa

Abstract

With the recent advances in video and 3D understanding, novel 4D spatio-temporal challenges fusing both concepts have emerged. Towards this direction, the Ego4D Episodic Memory Benchmark proposed a task for Visual Queries with 3D Localization (VQ3D). Given an egocentric video clip and an image crop depicting a query object, the goal is to localize the 3D position of the center of that query object with respect to the camera pose of a query frame. Current methods tackle the problem of VQ3D by lifting the 2D localization results of the sister task Visual Queries with 2D Localization (VQ2D) into a 3D reconstruction. Yet, we point out that the low number of Queries with Poses (QwP) from previous VQ3D methods severally hinders their overall success rate and highlights the need for further effort in 3D modeling to tackle the VQ3D task. In this work, we formalize a pipeline that better entangles 3D multiview geometry with 2D object retrieval from egocentric videos. We estimate more robust camera poses, leading to more successful object queries and substantially improved VQ3D performance. In practice, our method reaches a top-1 overall success rate of 86.36% on the Ego4D Episodic Memory Benchmark VQ3D, a 10× improvement over the previous state-of-the-art. In addition, we provide a complete empirical study highlighting the remaining challenges in VQ3D.

1. Introduction

The arrow of time is straight, unidirectional, flying from past to future, without any possibility of traveling back. Yet, Tulvin [30] identified the capacity of the human mind to recall past events as an exception to the irreversibility of the flow of time, defying nature's most fundamental law. Tulvin [31] defined *Episodic Memory* as the neuro-cognitive system that enables human beings to remember past experiences. *Episodic Memory* requires a sense of subjective time, autonoetic consciousness, and self, three neuro-cognitive components defining the human capability to think and reason [31]. In a race for better artificial intelligence, injecting



Figure 1. Visual Query with 3D Localization Task in Egocentric Videos. Given an egocentric video clip and an image crop depicting a *query object*, the goal is to localize the last time a *query object* was seen in the video and return the 3D displacement vector from the camera center of the *query frame* to the center of the object in 3D.

Episodic Memory abilities into our intelligent system would bring more humanity to those artificial machines, especially when assisting human beings in remembering past experiences.

Towards such efforts, the massive-scale dataset and benchmark suite Ego4D [15] introduced extensive challenges on *Episodic Memory* from egocentric videos, with the scope of browsing and searching past human experiences. Among those challenges, the task of Visual Queries (VQ) aimed at answering "Where was object X last seen in the video?", with X being a single image crop of an object, clearly visible and humanly identifiable. In particular, Visual Queries with 3D Localization (VQ3D) focuses on retrieving the relative 3D localization of a *query object* with respect to a current *query frame*, as illustrated in Figure 1.

The task of VQ3D arose from the natural progress in computer vision challenges, building on top of the latest development in image understanding [13,35], video understanding [15,29], and 3D geometric understanding [16,28].

Typically, VQ3D requires a frame-wise understanding of an egocentric video to localize objects in 2D images, coupled with a 3D scene understanding to lift the 2D localization into a 3D environment. Although most effort in Ego4D originates from the field of video understanding, little effort has been made to improve the meaningful 3D knowledge needed by VO3D methods.

In this work, we attempt to bridge the gap between video and 3D understanding in VQ3D. In particular, we develop a better 3D reconstruction module that produces more robust pose estimations for the frames of the egocentric videos. Furthermore, we derive a complete pipeline for VQ3D that better entangles the shared knowledge between egocentric videos and 3D, and we provide insight on how to further improve VQ3D methods. We summarize our contributions as follows:

- 1. We formalize a pipeline for the task of Visual Queries with 3D Localization (VQ3D) from egocentric videos that better entangles the 2D object retrieval output within the 3D scene information.
- 2. We show that better 3D reconstruction and camera pose estimation significantly increase the number of Queries with Poses (QwP), necessary to retrieve the localization of the *query objects*. Our pipeline reaches 86.36% in Overall Success Rate on the test set of the VQ3D task from the Ego4D Episodic Memory Benchmark server, a 10× improvement with respect to the previous state-of-the-art.
- We provide an empirical study of our pipeline, analyzing each of its modules, highlighting the parts that require further investigation, and pointing out future research directions.

2. Related Work

Our work relates to the topics of 3D geometric understanding and Episodic Memory from egocentric videos.

2.1. 3D Geometric Understanding

In order to localize the 3D position of objects from a video, we typically need to (i) reconstruct a 3D environment and/or (ii) localize those objects in 3D.

3D Reconstruction. Structure from Motion (SfM) is the process of estimating the 3D structure of a scene from a set of 2D images [28]. SfM typically reconstructs a sparse 3D point cloud and endows the images with poses and camera parameters. The Multi View Stereo (MVS) pipeline takes the posed calibrated images from SfM and produces a 3D dense point cloud reconstruction of the scene [28]. Similarly, Simultaneous Localization and Mapping (SLAM) methods reconstruct 3D scene from videos by leveraging

the temporal order of images from the video and generally aiming at real-time processing for embodied AI [20]. On one hand, SfM with MVS typically aims at high-quality reconstruction from unconstrained image structure, while on the other hand, SLAM focuses on real-time processing from temporal contiguous video frames. In this work, we rely on COLMAP [28] a general-purpose pipeline for 3D reconstruction based on SfM and MVS. We leverage its capability of structuring temporally ordered images, returning 3D camera poses, and a sparse 3D point cloud of the scene.

3D Object Detection. KITTI [14] introduced the task of localizing the 3D position, orientation, and extent of vehicles, bikes, and pedestrians from LIDAR point clouds in outdoor autonomous driving scenes. Recently, several works extended this task to exclusively consider images as inputs to localize objects of interest in 3D [4, 22, 27]. Similarly, ScanNet [10] proposed a task to localize objects with 3D bounding boxes in RGB-D indoor scans. Recently, ScanNet extended its localization task using natural language, leading to several efforts in language grounding [1, 8, 34], under similar motivation with episodic memory. In VQ3D, only the object's position is needed, defined as a simple 3D vector. As such, we instead rely on per-frame localization to lift per-frame localization into 3D.

2.2. Episodic Memory from Egocentric Videos

Egocentric Video Understanding. Egocentric video understanding is vital for many areas of research, such as vision, robotics, and augmented reality, but also with great difficulties. Much prior effort has been made to address challenges arising from a *first-person* view, such as activity recognition [19], detecting camera wearer's hands [3], and human body pose estimation [18]. The dynamics, motion blur, and unusual viewpoints caused by how egocentric videos are captured introduce overwhelming challenges. Still, a few efforts have been made for egocentric perception in a 3D context. [9] studied egocentric indoor localization based on the geometry of room layouts. EGO-SLAM [23] proposed a SLAM system for egocentric videos by solving it as an SfM problem over a temporal window.

Episodic Memory. Embodied Question Answering (EQA) [11, 12], is a special case of the video-language grounding task, where an embodied agent should answer language questions according to visual observations in 3D indoor environments. While EQA usually requires the model to give an answer [5] (*e.g.* language, video clip, *etc.*) to a language query, VQ3D considers image crops of objects as the query and predicts object displacement as output, which is more intuitive and fundamental for present computer vision techniques. Such a task setting is also strongly related to embodied AI problems [2,7,11], but they usually assume the poses are known and operate in stable simulators. Progress

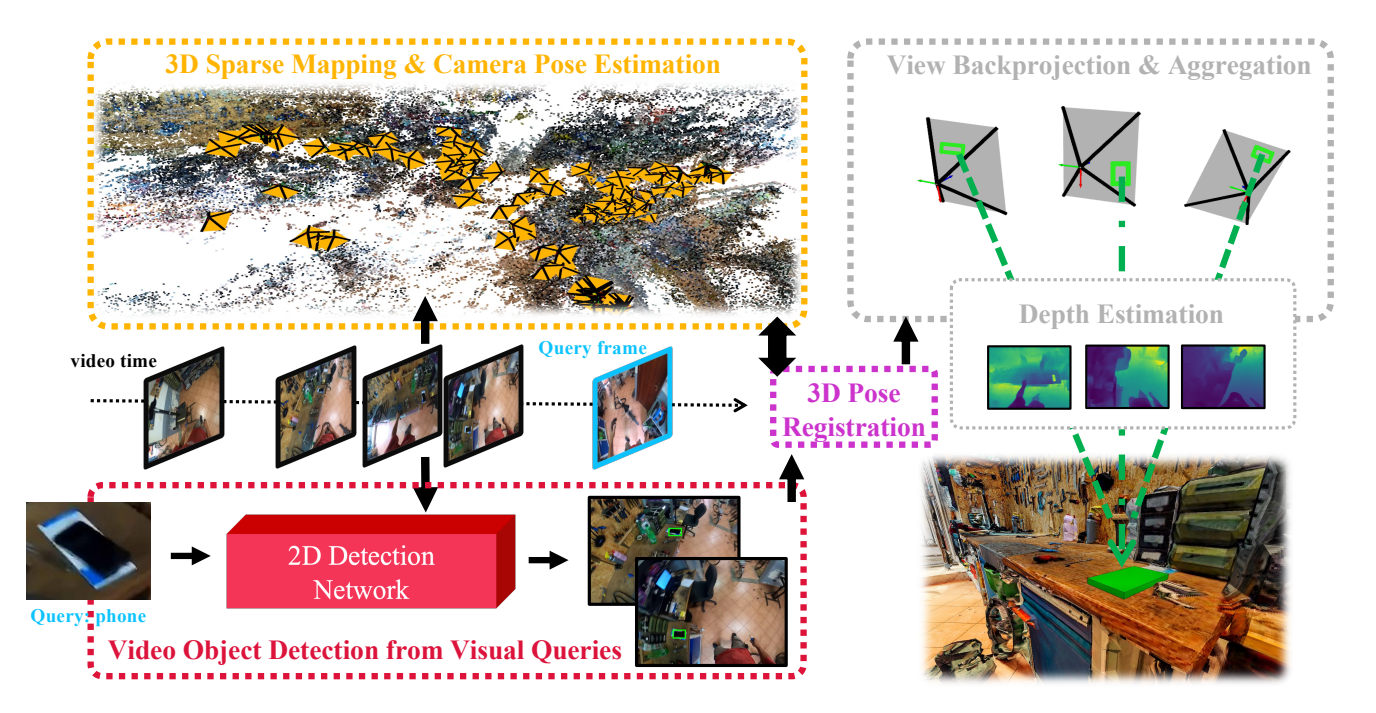


Figure 2. **Main Pipeline.** Our method reconstructs the 3D environment and retrieves the *query object* from each frame of the egocentric video. Then, we select the posed frames that successfully retrieve the *query object*, estimate the depth of these frames, and aggregate the 3D position of the retrieved object to form the final prediction.

in VQ3D has the potential to adapt embodied AI techniques into real-world applications.

3. Methodology

First, we formalize the VQ3D task as defined in the Ego4D Episodic Memory Benchmark [15]. Given an egocentric video \mathcal{V} , a query object o defined from a single visual crop v, and a query frame q, the objective is to estimate the relative displacement vector $\Delta d = (\Delta x, \Delta y, \Delta z)$ defining the 3D location where the query object o was last seen in the environment, with respect to the reference system defined by the 3D pose of the query frame q.

To localize a given image query in the video geometrically, we propose a multi-stage pipeline to entangle 2D information with 3D geometry. **First**, we perform a sparse 3D reconstruction with SfM [28], that estimate the 3D poses $\{T_0,...,T_N\}$ for the video frames and a sparse 3D map \mathcal{M} . Note that due to fast motion blur in egocentric videos, not all frames are actually assigned with a pose. **Second**, we feed the frames of an egocentric video \mathcal{V} and the visual crop v of a query object o to a model that retrieves response frames $\{k_{p_0}, k_{p_1}....\}$ with corresponding 2D bounding boxes $\{b_{p_0}, b_{p_1}....\}$ of the query object o. **Third**, for the response frames that are missing 3D poses, we register them with the sparse 3D map \mathcal{M} . Note that still, some response frames with fast motion blur might not be assigned with a pose. **Finally**, for each response

frames p_i , we estimate the depth and backproject the object centroid in 3D, to recover the relative displacement vector $\Delta d_{p_i} = (\Delta x_{p_i}, \Delta y_{p_i}, \Delta z_{p_i})$ with respect to the query frame q. The final relative displacement vector Δd is aggregated from the 3D displacements Δd_{p_i} per response frame p_i . Figure 2 illustrates an overview of our pipeline.

3.1. 3D Sparse Mapping & Camera Pose Estimation

Estimating the camera poses from egocentric videos is difficult, yet essential for high-level tasks. To recover camera poses, the baseline from Ego4D [15] tried to extract the features and match them between the sampled renderings of Matterport Scan and selected frames from the egocentric videos. However, there is a domain gap between egocentric videos and Matterport scans, as shown in Figure 3, and already observed in previous works [6, 26]. As a result, the Ego4D [15] baseline mostly fails to match video frames, leading to inaccurate 3D reconstruction, low number of Query with Poses (QwP), and low performance in the VQ3D metrics.

To alleviate this issue, we propose to use Structure-from-Motion (SfM) techniques to estimate the camera poses among the video frames directly. In this way, we no longer need to worry about the inconsistency between scanned frames and video frames, but we also get rid of the strong assumption that there must be an existing 3D scan of the video scene. This saves a lot of computing power and resources



Figure 3. Egocentric Videos and Matterport Scan. We show illustrations of the domain gap between Matterport Scan and real scenes. MP Scan may have different illumination, scene appearance, and missing/low-quality scans. Egocentric videos are usually dynamic, free of view (FOV), and have fast motion blur, bringing great challenges for 3D reconstruction and localization.

for scan creation and makes our method easy to migrate and work in real-world applications.

Specifically, we build our SfM module upon the widely popular COLMAP [28] for 3D sparse mapping and camera pose estimation. Given an egocentric video $\mathcal V$ with frames $\{k_i, i \in \mathcal{I}\}$ where \mathcal{I} is the total number of frames, we first extract the features of the frames and match them among the video frames. Since the video frames are ordered, we adopt the sequential matching functionality from COLMAP, which leads to a fast SfM with acceptable quality for the thousands of images to structure. For each frame k_i , COLMAP performs a coarse matching with its temporal neighboring frames $\{k_{i-\frac{w}{2}},...,k_{i+\frac{w}{2}}\}$ in a window size of w. It creates a scene graph that matches temporally contiguous images. We feed our video frames with the scene graphs into our COLMAP solver, which reconstructs a sparse 3D map \mathcal{M} from the video key frames $\{k_{m_0}, k_{m_1}, ...\}$ that were successfully registered. Figure 5 depicts the details of this first stage. We highlight the video key frames as orange in Figures 2 and 5. The map \mathcal{M} with sparse feature points and pose images will be our input for second-stage image localization later on.

3.2. Video Object Detection from Visual Queries

The Video Object Detection from Visual Queries module aims at localizing temporally and spatially a query object o defined with a single visual crop v. The VQ3D baseline from Ego4D [15] uses an existing pipeline developed from the VQ2D baseline, based on object detection and tracking.

However, we argue that lifting VQ2D results to 3D might

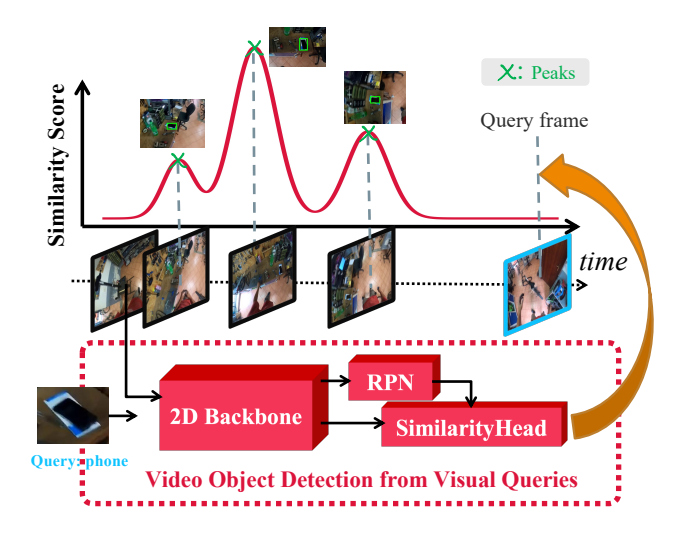


Figure 4. Our 2D Object Retrieval Module. The 2D Backbone \mathcal{F} extracts the features for both query object o and the input video stream. A pre-trained RPN [25] network with ROI-Align [17] operation is then used to generate bbox proposals and visual features. A Siamese head is trained to evaluate the similarity between query object features and bbox proposal features. At inference time, the peak responses in the score signals will be selected as our response frames.

not be optimal. We find the tracking module cumbersome and prone to error, providing blurry frames and uncertain tracklets subject to drift. Therefore, we revisit the VQ2D [15, 33] implementation by pruning the tracker and coupling the detector more tightly with the 3D modules.

Formally, given a static visual crop v specifying the query object o, and an egocentric video \mathcal{V} with query frame indexed k_q , our goal is to find out the *response* frames from the previous video stream $\{k_0, ..., k_q\}$ that contains the query object o. As shown in Figure 4, we use a pretrained 2D backbone to generate bounding box proposals $\{b_1, ..., b_N\}$ with corresponding features $\{\mathcal{F}(b_1),...,\mathcal{F}(b_N)\}$. Then, a Siamese Head Scorer is trained to evaluate the similarity between these features and the query feature $\mathcal{F}(v)$.

At inference time, the 2D network provides a similarity score for each frame indexed $\{k_0,...,k_q\}$ before the query frame, as shown on the plot at the top of Figure 4. After smoothing the scores, we identify the peaks larger than a given threshold and select our response frames accordingly. We hypothesize that a peak signal indicates higher confidence for the query object o to be present in the video frame, and should identify high-quality images with more accurate bounding box predictions. Finally, we couple the peak response frames with their corresponding top-1 bounding box proposal as follows: $\{(k_{p_0}, b_{p_0}), (k_{p_1}, b_{p_1}), \dots, \}$.

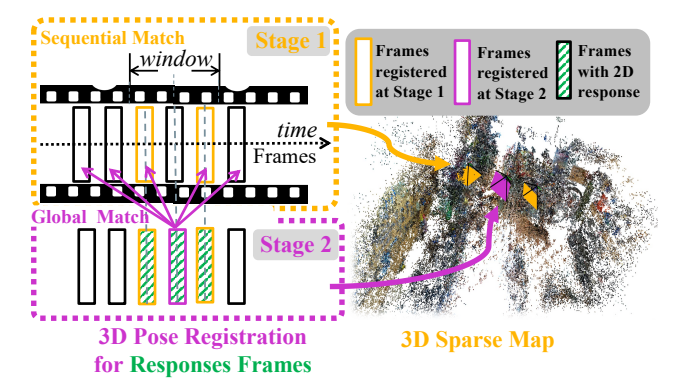


Figure 5. Two-stage approach for camera pose estimation At Stage 1, we match and register video frames to \mathcal{M} within a sliding window. The frames in orange are successfully localized to the 3D map \mathcal{M} . At Stage 2, once we know the 2D response frames with object presence, we pick the unregistered responses (purple frames), match them with all the frames exhaustively, and manage to register them into \mathcal{M} with relaxed conditions.

3.3. 3D Pose Registration for Responses Frames

The VQ3D baseline from Ego4D [15] associates 2D response frames with 3D reconstruction, by indexing the 3D map \mathcal{M} and checking if the response frames are registered. That is, if there exists k_{m_j} in map \mathcal{M} and k_{p_i} in response frames \mathbf{p} such that $m_j = p_i$, posed view of object o is found.

However, since egocentric videos are challenging for camera pose estimation (see Figure 3), many response frames fail to find any matches in registered temporal neighbors and cannot be registered into the 3D map \mathcal{M} . The lack of responses can lead to inaccurate 3D displacement prediction and even impede any possible prediction.

To address this issue, in addition to the first stage of reconstruction and localization, we propose an additional second stage of reconstruction for a more robust camera pose estimation for the responses. The two stages of our 3D process pipeline are put together in Figure 5. In the second pass, the registration procedure is guided by registering the missing responses. For those valid 2D responses $\{k_{p_0},k_{p_1},\ldots\}$ input from 2D object retrieval, if we fail to index response k_{p_i} in the 3D map \mathcal{M} , we perform an exhaustive global matching for k_{p_i} with all the registered frames $\{k_{m_0}, k_{m_1}, ...\}$. This follows the observation that humans may visit similar locations again in indoor activities, so frames with similar appearances in a close place may be far away temporally. Additionally, since these responses are essential for our task, we relax the conditions for image registration and triangulation after the global matching, sacrificing some localization accuracy to trade-off for more posed response frames. Note that we check the query frame in Stage 2 following a similar process.

After a final global bundle adjustment that refines the

reconstruction, for every registered 2D response k_{p_i} we associate its 3D camera pose T_{p_i} as our 4D scene memory for object $o: \{(k_{p_0}, b_{p_0}, T_{p_0}), (k_{p_1}, b_{p_1}, T_{p_1}), \ldots\}$.

3.4. View Backprojection & Aggregation

Finally, for each posed response frame, we estimate the 3D position for the center of the 2D bounding box. We estimate the depth maps for the posed response frames using a pretrained monocular depth estimation network DPT [24]. With paired response k_{p_i} and bounding box b_{p_i} together, we predict the depth d of the object o as the depth value of its centroid in the depth map. The backprojection of the 2D position into a 3D displacement vector $[x_i, y_i, z_i]$ for posed view k_{p_i} is given in Equation (1), where u_i, v_i correspond to the centroid of the bounding box b_{p_i} and K is the intrinsic parameters of the camera estimated by COLMAP. A visual description of this module is shown on the right side of Figure 2.

$$\begin{bmatrix} x_i \\ y_i \\ z_i \end{bmatrix} = T_{p_i} dK^{-1} \begin{bmatrix} u_i \\ v_i \\ 1 \end{bmatrix}$$
 (1)

Unlike the Ego4D baseline [15] that only uses the last tracking response, we aggregate information from multiple points of view to localize the query object o, which leads to a more accurate estimation of the displacement vector Δd , more robust to noisy posed views. We make a simple assumption here that the recent multiple appearances of an object in a short video clip should be geometrically close to each other in the world coordinate system, in particular since the object tends to be static without extensive movement. We defined our aggregation function $\mathcal A$ in Equation (2). Practically, we experiment with average and median operations for the aggregation operator $\mathcal A$ between the 3D displacement vectors from the posed response frames.

$$[\hat{x}, \hat{y}, \hat{z}] = \mathcal{A}([x_0, y_0, z_0], ..., [x_i, y_i, z_i])$$
 (2)

4. Experiments

4.1. Ego4D VQ3D Benchmark

Ego4D [15] is a massive-scale egocentric video dataset and benchmark suite. As a part of the episodic memory benchmark, the VQ3D task contains 164, 44 and 69 video clips for train, validation, and test set, respectively. There are 164 and 264 visual queries in the validation and test sets, respectively. The video clips typically last from 5 to 10 minutes. All those video clips are recorded in indoor scenes that have been scanned with Matterport devices before. The ground-truth 3D locations of the objects are annotated by volunteers in the Matterport scans.

•		Validation set				Test set					
Method	Improvements	Succ%↑	Succ*%↑	L2↓	Angle↓	QwP%↑	Succ%↑	Succ*%↑	L2↓	Angle↓	QwP%↑
Ego4D [15]	Baseline	1.22	30.77	5.98	1.60	1.83	8.71	51.47	4.93	1.23	15.15
Ours	+ Sequential 3D Registation	67.07	89.93	2.20	0.99	74.39	73.48	85.83	2.39	0.72	85.99
	+ Detection peaks w/o tracking	71.34	94.84	2.05	0.94	75.00	77.65	90.35	2.22	0.68	87.12
	+ 2D guided 3D registration	76.22	94.94	2.06	0.96	80.49	81.06	90.35	2.20	0.66	90.53
	+ Multiview Mean	77.44	96.84	1.78	0.89	80.49	86.36	95.37	1.94	0.60	90.53

Table 1. **Main Results.** We show our results on the validation and test sets of the VQ3D task from the Ego4D Episodic Memory Benchmark. We also highlight the performance change with and without our main modules.

4.2. Experimental Setup

We customize COLMAP [28] and explore the proper hyperparameters for egocentric videos empirically. In the two-stage reconstruction, we use the sequential matcher and vocabulary tree matcher, for the first and second stage, respectively. We adopt Faster-RCNN [25] as our 2D feature extraction backbone, a pre-trained Region Proposal Network (RPN) [25] with a Feature Pyramid Network (FPN) [21] followed by ROI Align operation [17] as the proposal and feature generator. We utilize the *median_filter* and *find_peaks* function from Scipy [32] library to select responses from similarity scores. We adopt the pretrained DPT [24] network pretrained for depth estimation.

4.3. Metrics

For a fair comparison, we use the same metrics as defined by Ego4D's baseline [15]. Angle corresponds to the angular error in radians and L2 corresponds to the distance error in meters using the root mean square error (RMSE):

$$L2 = ||t_s - \hat{t}_s||_2 \tag{3}$$

angle =
$$acos(\frac{v_Q^T}{\|v_Q\|_2} \cdot \frac{\hat{v}_Q^T}{\|\hat{v}_Q\|_2})$$
 (4)

where t_s and \hat{t}_s are the ground-truth location and predicted location, respectively. v_Q and \hat{v}_Q are the ground truth location and predicted location in the query frame's coordinate system. QwP represents the query ratio for which we have pose estimation for both the response frames and the query frame. The success metric is formulated as follows:

$$succ = ||c_m - \hat{t}_s||_2 < 6 \times (||c_1 - c_2||_2 + exp^{-m_{diag}})$$
 (5)

where c_1 and c_2 are the centroids of the two ground-truth bounding box annotations, c_m is the mid-centroid between c_1 and c_2 , m_{diag} is the average diagonal length of the two boxes. The success rate with star * means the success metric computed only for queries with associated pose estimates.

4.4. VQ3D Results

We show our main results in Table 1. We observe significant improvements in both the validation set and test set

for all the metrics. For the overall success rate, our revised pipeline paved the way for substantial improvement. The success rate goes from 1.22% to 77.44% in the validation set and from 8.71% to 86.36% in the test set. We describe next the main findings from the results.

More poses of the video frames. As hypothesized, the low success rate in Ego4D was mainly due to the low Queries with Poses (QwP) ratio. Actually, we can directly infer that QwP is the upper bound of the most important metric, the overall success rate. Without the frames poses, 3D displacement estimation is not possible. The low QwP destroying their performance is caused by their method for camera pose estimation, trying to do feature matching crossing a huge domain gap in simulation and real scenes, as can be scene in the first line in our results in Table 1.

Important images re-registration. Further investigation can showcase that the proposed 2D responses guided image registration effectively improves camera pose estimation for keyframes. The 5.49% improvement on QwP boosts the overall success rate by 4.88% on the validation set thanks to more registered keyframes (Tb. 3). Also, we notice that the absolute success rate in validation and test set has big differences, comparing Ego4D's 1.22% with 8.71%, our 77.44% with 86.36%. This is because ego videos are usually in high variance. Egocentric videos recorded in different scenes and activities may have totally different difficulties in pose estimation.

Object detection for frames selection. Moreover, around 4% improvement in the overall success and success* by selecting the peaks from detection verifies our analysis that using the last response from tracking is risky and high detection peaks suggest high confidence in the clear presence of an object. While the last frame from the response track may be blurry or on the border of images with high uncertainty.

Multi-View aggregation. We finally note that our multiview aggregation strategy gives a 5.30% boost on the test set. And it gets a remarkable reduction for the metrics caring about "accuracy", i.e., L2 and angle errors on both sets. This result implies the importance of fusing multi-view information, especially in reducing the noise and uncertainty for more accurate object 3D localization.

Module	Method	Succ%↑	Succ*%↑	L2↓	Angle↓	QwP%↑
(3.1) 3D Sparse Mapping & Camera Pose Estimation	Sim2Real [15] Sequential 3D Registration	1.22 67.07	30.77 89.93	5.98 2.20	1.60 0.99	1.83 74.39
(3.2) Video Object Detection from Visual Queries	Detection and Tracking [15] Detection Peaks Groundtruth Detection	67.07 71.34 71.95	89.93 94.84 98.59	2.20 2.05 1.47	0.99 0.94 0.67	74.39 75.00 73.17
(3.3) 3D Pose Registration for Responses Frames	Direct Index [15] 2D Guided 3D registration	71.34 76.22	94.84 94.94	2.05 2.06	0.94 0.96	75.00 80.49
(3.4) View Backprojection & Aggregation	Last Response [15] Multiview Median Multiview Mean	76.22 76.22 77.44	94.94 95.57 96.84	2.06 1.82 1.78	0.96 0.88 0.89	80.49 80.49 80.49

Table 2. **Ablation study**. We show a step-by-step ablation study for our four main modules on the validation set of VQ3D benchmark. We find the best strategy for each module and then move to the next sequentially. The modules below will inherit the **bold text** setting from the modules above, while the modules above will use the default setting from the modules below it, *i.e.*, Ego4D's strategy on the first row of each part.

5. Analysis

We provide an empirical study of our pipeline with more details to review current techniques and highlight insights for the future. We perform a step-by-step ablation study in Table 2 for our four modules, on the validation set of VQ3D benchmark. When we find an optimal setting for a module, we configure and fix it to explore the best strategy for the next module.

5.1. Camera Pose Estimation

From our experiment result, camera pose estimation is the most crucial part for VQ3D task. Here we ablate our first and third modules related to our two-stage camera pose estimation as shown in Part (3.1) and Part (3.3) of Table 2.

For the first module, 3D reconstruction and Localization, Sim2Real is the strategy of Ego4D, which tries to register real video frames to simulated Matterport scans. With our sequential matching based SfM in first-stage of registration, which runs the reconstruction just for video clips for short-term camera pose estimation, We witness significant 65.85% lift, mainly contributed by 72.56% improvements from QwP in terms of overall success rate. In terms of accuracy, the reduction from 5.98 to 2.20 in L2 loss and the decrease from 1.6 to 0.99 in angular error suggest that an on-the-shelf SfM can be an appropriate workaround for egocentric localization.

Regarding our second stage of image registration integrated into 3D-2D association module, we also observe a similar phenomenon that the improvement in QwP is proportional to the improvement in overall success, comparing the delta of 5.49% with 4.88%. The performance gain comes from an increased number of registered responses in Table 3

Additionally, we find a minor drop in L2 and angle performance since we loose the registration conditions for response

Method	Frames w/ Pose	Response Frames w/ Pose	QwP%↑	Succ%↑
Ego4D-Sim2Real [15]	4,848	267	1.83	1.83
1 Stage Registration	79,627	2,273	75.00	71.34
2 Stage Registration	83,063	2,390	80.49	76.22

Table 3. Analysis on the number of Query with Poses (QwP). We report the number of camera frames with poses and response frames with poses on the validation set. In total, there are 96,037 frames in the 44 video clips of the validation set. The single stage approach already increase the number of frames with pose and response frame with poses by a factor of 20, while the 2-stage approach increase it even more.

frames, but we think such a trade-off is acceptable.

5.2. Video Object Detection

Part (3.2) of Table 2 gives the analysis for Video Object Detection. Notice we use the last response strategy here, which selects only one response frame nearest to the query frame for prediction. Also, since we are changing the selected responses here, the Queries with Poses (QwP) ratio can be slightly different.

"Detection and Tracking" is Ego4D's strategy to localize the object in 2D. They pick the detection response peak closest to query frame (Figure 4), then run the tracker forward and backward to get the response track. Their motivation is that last frame from response track should be exactly the answer of "where did I last see object X?" However, except for the time and computation overheads, the last track is when we are about to lose track of the object, the response can be blurry and the object can be far away from the center of the frame, raising difficulties for backprojection to 3D.

Our "Detection Peaks" strategy only considers the peak response from the similarity score map in Figure 4. Here



Figure 6. **Visualization of 2D responses and 3D Localization.** We visualize the 2D response detection on the top row with the corresponding 3D localization below. We backproject the response frame to an example Matterport scan using estimated depth map and camera poses. The highlighted area is backprojection, and the faded area is groundtruth scene scan. **For query (a)**, our object detection module gives the correct bbox while the tracking result from Ego4D has shifted, leading to better 3D localization. **For query (b)**, although our method has an inexact 2D response, we still perform better in L2 metric because of better pose estimation.

we care more about the confidence and precision of "where did I last see object X?". With similar QwP, we boost the overall success from 67.07% to 71.34%, also for L2 and angle accuracies.

In addition, as a subset of VQ2D data, VQ3D benchmark has the ground truth tracking annotations for the query object's last appearance. We also evaluate our pipeline by substituting the responses as ground truth tracking. We find that ground truth 2D annotations can significantly reduce the object localization shift, with L2 reduced by 0.58 meters and angular error reduced by 0.27. However, the overall success rate is only 0.61% higher than Detection Peaks though it's the highest. This indicates that the 2D object retrieval module is almost saturated compared to our camera pose estimation. Even the current Siamese detector still lacks 2D detection accuracy [15,33], we are close to the upper bound of potential improvements gained from 2D object retrieval.

For instance, a wrong localization of another object on the table may be catastrophic for 2D metrics, but it is likely to be treated as correct localization in 3D metrics, just with a slightly larger L2 distance, as we observed in Figure 6 (b). Here the error is dominated by inexact/missing camera pose estimation rather than 2D object retrieval. This could be an interesting direction for follow-up works to explore.

5.3. Backprojection and Aggregation

We study how to select posed response frames in Part (3.4) of Table 2. The simplest way to do backprojection for object *o* in 3D is taking one single response for Equation (1). However, since our pipeline is multi-stage, prediction

from one single frame could be fragile to the errors we accumulated in each module. Aggregating 3D displacements predicted from multiview strengthens the 3D precision as we have found in the L2 and angle column from Table 2 and Table 1. Especially, more pronounced improvement in overall success is observed on the test set in a magnitude of 5.3%. We find that both aggregation functions, $\mathcal{A}=mean$ and $\mathcal{A}=median$ can improve the performance, with $\mathcal{A}=mean$ performing slightly better in terms of overall success rate

For depth estimation, since we have multiviews from known poses, the optional approach is to triangulate those 2D bounding box centroids. But related VQ2D works [15, 33] show that some false positives are in the 2D detection results, which may harm the optimization of 3D triangulation. Since Ego4D [15] has shown that depth estimation from DPT [24] is comparable to groundtruth depth quantitatively and qualitatively, we follow the same settings with DPT here.

6. Conclusions and Future Works

In this work, we reformalize the VQ3D task clearly and build a modular pipeline, allowing for substantial improvements on Ego4D VQ3D benchmark. An abundance of experiments are performed to validate the proposed methodology, including different ablations on all the components of the work. Despite the substantial effort put forth in this project to address the VQ3D task, we believe it is only the first step in this direction and aimed to further push the research in 4D understanding direction. Another important future possibility is the deployment of the successful methods and

strategies followed in this project for the classical vision tasks in video understanding. The utilization of 3D knowledge in such setups can prove to be advantageous.

References

- [1] Panos Achlioptas, Ahmed Abdelreheem, Fei Xia, Mohamed Elhoseiny, and Leonidas Guibas. Referit3d: Neural listeners for fine-grained 3d object identification in real-world scenes. In *European Conference on Computer Vision*, pages 422–440. Springer, 2020. 2
- [2] Peter Anderson, Qi Wu, Damien Teney, Jake Bruce, Mark Johnson, Niko Sünderhauf, Ian Reid, Stephen Gould, and Anton Van Den Hengel. Vision-and-language navigation: Interpreting visually-grounded navigation instructions in real environments. In *Proceedings of the IEEE conference on* computer vision and pattern recognition, pages 3674–3683, 2018. 2
- [3] Sven Bambach, Stefan Lee, David J Crandall, and Chen Yu. Lending a hand: Detecting hands and recognizing activities in complex egocentric interactions. In *Proceedings of the IEEE international conference on computer vision*, pages 1949–1957, 2015. 2
- [4] Wentao Bao, Bin Xu, and Zhenzhong Chen. Monofenet: Monocular 3d object detection with feature enhancement networks. *IEEE Transactions on Image Processing*, 29:2753– 2765, 2019.
- [5] Leonard Bärmann and Alex Waibel. Where did i leave my keys?-episodic-memory-based question answering on egocentric videos. In *Proceedings of the IEEE/CVF Conference on Computer Vision and Pattern Recognition*, pages 1560–1568, 2022. 2
- [6] Arunkumar Byravan, Jan Humplik, Leonard Hasenclever, Arthur Brussee, Francesco Nori, Tuomas Haarnoja, Ben Moran, Steven Bohez, Fereshteh Sadeghi, Bojan Vujatovic, et al. Nerf2real: Sim2real transfer of vision-guided bipedal motion skills using neural radiance fields. arXiv preprint arXiv:2210.04932, 2022. 3
- [7] Devendra Singh Chaplot, Dhiraj Gandhi, Saurabh Gupta, Abhinav Gupta, and Ruslan Salakhutdinov. Learning to explore using active neural slam. arXiv preprint arXiv:2004.05155, 2020. 2
- [8] Dave Zhenyu Chen, Angel X Chang, and Matthias Nießner. Scanrefer: 3d object localization in rgb-d scans using natural language. In *European Conference on Computer Vision*, pages 202–221. Springer, 2020. 2
- [9] Xiaowei Chen and Guoliang Fan. Egocentric indoor localization from coplanar two-line room layouts. In *Proceedings of the IEEE/CVF Conference on Computer Vision and Pattern Recognition*, pages 1549–1559, 2022.
- [10] Angela Dai, Angel X. Chang, Manolis Savva, Maciej Halber, Thomas Funkhouser, and Matthias Nießner. Scannet: Richlyannotated 3d reconstructions of indoor scenes. In *Proc. Com*puter Vision and Pattern Recognition (CVPR), IEEE, 2017.
- [11] Abhishek Das, Samyak Datta, Georgia Gkioxari, Stefan Lee, Devi Parikh, and Dhruv Batra. Embodied question answering.

- In Proceedings of the IEEE Conference on Computer Vision and Pattern Recognition, pages 1–10, 2018. 2
- [12] Samyak Datta, Sameer Dharur, Vincent Cartillier, Ruta Desai, Mukul Khanna, Dhruv Batra, and Devi Parikh. Episodic memory question answering. In *Proceedings of the IEEE/CVF* Conference on Computer Vision and Pattern Recognition, pages 19119–19128, 2022. 2
- [13] Jia Deng, Wei Dong, Richard Socher, Li-Jia Li, Kai Li, and Li Fei-Fei. Imagenet: A large-scale hierarchical image database. In Computer Vision and Pattern Recognition, 2009. CVPR 2009. IEEE Conference on, pages 248–255. IEEE, 2009. 1
- [14] Andreas Geiger, Philip Lenz, and Raquel Urtasun. Are we ready for autonomous driving? the kitti vision benchmark suite. In Conference on Computer Vision and Pattern Recognition (CVPR), 2012.
- [15] Kristen Grauman, Andrew Westbury, Eugene Byrne, Zachary Chavis, Antonino Furnari, Rohit Girdhar, Jackson Hamburger, Hao Jiang, Miao Liu, Xingyu Liu, et al. Ego4d: Around the world in 3,000 hours of egocentric video. In *Proceedings of the IEEE/CVF Conference on Computer Vision and Pattern Recognition*, pages 18995–19012, 2022. 1, 3, 4, 5, 6, 7, 8, 11, 12, 13
- [16] Abdullah Hamdi, Silvio Giancola, and Bernard Ghanem. Mvtn: Multi-view transformation network for 3d shape recognition. In Proceedings of the IEEE/CVF International Conference on Computer Vision (ICCV), pages 1–11, October 2021.
- [17] Kaiming He, Georgia Gkioxari, Piotr Dollár, and Ross Girshick. Mask r-cnn. In *Proceedings of the IEEE international conference on computer vision*, pages 2961–2969, 2017. 4, 6
- [18] Hao Jiang and Kristen Grauman. Seeing invisible poses: Estimating 3d body pose from egocentric video. In 2017 IEEE Conference on Computer Vision and Pattern Recognition (CVPR), pages 3501–3509. IEEE, 2017. 2
- [19] Evangelos Kazakos, Arsha Nagrani, Andrew Zisserman, and Dima Damen. Epic-fusion: Audio-visual temporal binding for egocentric action recognition. In *Proceedings of the IEEE/CVF International Conference on Computer Vision*, pages 5492–5501, 2019. 2
- [20] Mathieu Labbé and François Michaud. Rtab-map as an opensource lidar and visual simultaneous localization and mapping library for large-scale and long-term online operation. *Journal* of Field Robotics, 36(2):416–446, 2019.
- [21] Tsung-Yi Lin, Piotr Dollár, Ross Girshick, Kaiming He, Bharath Hariharan, and Serge Belongie. Feature pyramid networks for object detection. In *Proceedings of the IEEE* conference on computer vision and pattern recognition, pages 2117–2125, 2017. 6
- [22] Shujie Luo, Hang Dai, Ling Shao, and Yong Ding. M3dssd: Monocular 3d single stage object detector. In *Proceedings of the IEEE/CVF Conference on Computer Vision and Pattern Recognition*, pages 6145–6154, 2021.
- [23] Suvam Patra, Kartikeya Gupta, Faran Ahmad, Chetan Arora, and Subhashis Banerjee. Ego-slam: A robust monocular slam for egocentric videos. In 2019 IEEE Winter Conference on Applications of Computer Vision (WACV), pages 31–40. IEEE, 2019. 2

- [24] René Ranftl, Alexey Bochkovskiy, and Vladlen Koltun. Vision transformers for dense prediction. In *Proceedings of the IEEE/CVF International Conference on Computer Vision*, pages 12179–12188, 2021. 5, 6, 8
- [25] Shaoqing Ren, Kaiming He, Ross Girshick, and Jian Sun. Faster r-cnn: Towards real-time object detection with region proposal networks. Advances in neural information processing systems, 28, 2015. 4, 6
- [26] Marco Rosano, Antonino Furnari, Luigi Gulino, and Giovanni Maria Farinella. On embodied visual navigation in real environments through habitat. In 2020 25th International Conference on Pattern Recognition (ICPR), pages 9740–9747. IEEE, 2021. 3
- [27] Danila Rukhovich, Anna Vorontsova, and Anton Konushin. Imvoxelnet: Image to voxels projection for monocular and multi-view general-purpose 3d object detection. In *Proceedings of the IEEE/CVF Winter Conference on Applications of Computer Vision*, pages 2397–2406, 2022. 2
- [28] Johannes Lutz Schönberger and Jan-Michael Frahm. Structure-from-motion revisited. In Conference on Computer Vision and Pattern Recognition (CVPR), 2016. 1, 2, 3, 4, 6, 13
- [29] Mattia Soldan, Alejandro Pardo, Juan León Alcázar, Fabian Caba, Chen Zhao, Silvio Giancola, and Bernard Ghanem. Mad: A scalable dataset for language grounding in videos from movie audio descriptions. In *Proceedings of the IEEE/CVF Conference on Computer Vision and Pattern Recognition*, pages 5026–5035, 2022. 1
- [30] Endel Tulving. Episodic and semantic memory. 1972. 1
- [31] Endel Tulving. Episodic memory: From mind to brain. *Annual review of psychology*, 53(1):1–25, 2002. 1
- [32] Pauli Virtanen, Ralf Gommers, Travis E. Oliphant, Matt Haberland, Tyler Reddy, David Cournapeau, Evgeni Burovski, Pearu Peterson, Warren Weckesser, Jonathan Bright, Stéfan J. van der Walt, Matthew Brett, Joshua Wilson, K. Jarrod Millman, Nikolay Mayorov, Andrew R. J. Nelson, Eric Jones, Robert Kern, Eric Larson, C J Carey, İlhan Polat, Yu Feng, Eric W. Moore, Jake VanderPlas, Denis Laxalde, Josef Perktold, Robert Cimrman, Ian Henriksen, E. A. Quintero, Charles R. Harris, Anne M. Archibald, Antônio H. Ribeiro, Fabian Pedregosa, Paul van Mulbregt, and SciPy 1.0 Contributors. SciPy 1.0: Fundamental Algorithms for Scientific Computing in Python. Nature Methods, 17:261–272, 2020. 6
- [33] Mengmeng Xu, Cheng-Yang Fu, Yanghao Li, Bernard Ghanem, Juan-Manuel Perez-Rua, and Tao Xiang. Negative frames matter in egocentric visual query 2d localization. arXiv preprint arXiv:2208.01949, 2022. 4, 8
- [34] Lichen Zhao, Daigang Cai, Lu Sheng, and Dong Xu. 3dvg-transformer: Relation modeling for visual grounding on point clouds. In *Proceedings of the IEEE/CVF International Conference on Computer Vision*, pages 2928–2937, 2021. 2
- [35] Zhong-Qiu Zhao, Peng Zheng, Shou-tao Xu, and Xin-dong Wu. Object detection with deep learning: A review. IEEE transactions on neural networks and learning systems, 30(11):3212–3232, 2019.

A. Supplementary Results

A.1. Validation Set

We provide detailed results in Table 4 for all the modules with different method settings. *Groundtruth Track* stands for the groundtruth tracking result provided by Ego4D VQ2D annotations, a temporal consecutive frame set showing the object's last appearance. The groundtruth response track is specified as r, which is a temporally contiguous set of bounding boxes surrounding the object o in each frame:

$$r = \{r_s, r_{s+1}, ..., r_{e-1}, r_e\},\$$

where s is the frame where the object o (at least partially) enters the camera wearer's field of view, e is the frame where the object exits the camera wearer's field of view, and r_i is a bounding box (x,y,w,h) in frame i. If the object appears multiple times in the video, the response only refers to the 'most recent appearance' of the object in the past, i.e., the response track which minimizes $q-r_e$ with $q>r_e$.

Therefore, we don't have groundtruth detection annotations for all the frames in Ego4D, so we can't evaluate our proposed 2D response detection in this work.

A.2. Test Set

We provide detailed results in Table 5 for all the modules with different method settings. We can find the full validation and test set results also follow our observation and discussion in the paper.

B. More Visualizations

Though we don't have enough camera poses from Ego4D [15] baseline, we instead provide 2D and 3D visualization from our method. We visualize our results in four scenes, *Baker* (Figure 7), *Bike* (Figure 8), *Carpenter* (Figure 9), *Mechanic* (Figure 10).

- 1. For 2D visualization, we use white to represent our predictions and green to represent the groundtruth.
- 2. For 2D visualization, because we only have access to the groundtruth response track instead of groundtruth detection, we don't have groundtruth 2D bbox in some cases but only our own prediction bbox in white.
- 3. For 3D visualization, note that we actually don't know the size and rotation of 3D bbox during prediction. But we use the size and rotation from groundtruth annotations during our visualization with our predicted 3D vector (x, y, z) as the center of 3D bbox.

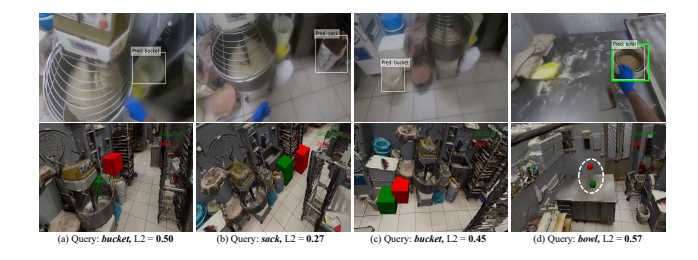


Figure 7. Scene Baker In this scene, we find that the overall L2 distance is small when the objects are large because large objects are easy to detect and localize in 3D.

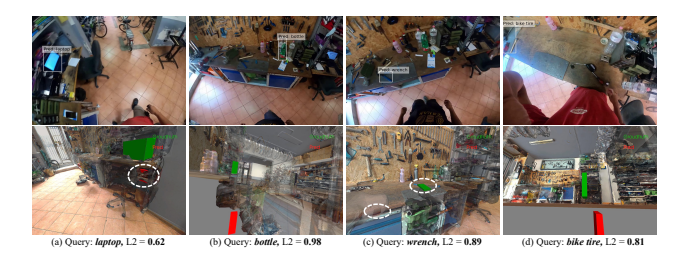


Figure 8. **Scene Bike** In this scene, the error of the first three queries comes from inaccurate camera pose estimation, whereas the last one comes from both wrong detection and wrong camera pose.



Figure 9. **Scene Carpenter** Videos in this scene are very challenging because the illumination of this house is poor and changes all the time. Some of our predictions for queries from this scene are very bad that even out of the scene bound.



Figure 10. **Scene Mechanic** We observe the same phenomenon as in Figure 7 that large objects tend to be more precise, not only 2D detection but also 3D localization.

VQ3D-Val	Succ%↑	Succ*%↑	L2↓	Angle↓	QwP%↑	(3.1) 3D Sparse Mapping & (3.2) Video Object Detection Camera Pose Estimation from Visual Queries		(3.3) 3D pose Registration for Response Frames	(3.4) View Backprojection & Aggregation
Ego4D [15]	1.22	30.77	5.98	1.60	1.83	Sim2Real	Detection + Tracking	Direct Index	Last Response
Ours	67.07	89.93	2.20	0.99	74.39	Sequential 3D Registration	Detection+Tracking	Direct Index	Last Response
Ours	68.29	92.09	2.17	0.97	74.39	Sequential 3D Registration	Detection+Tracking	Direct Index	MultiView Median
Ours	68.29	92.09	2.15	0.97	74.39	Sequential 3D Registration	Detection+Tracking	Direct Index	MultiView Mean
Ours	73.17	89.86	2.22	1.01	81.10	Sequential 3D Registration	Detection+Tracking	2D Guided 3D registration	Last Response
Ours	74.39	92.57	2.13	0.99	81.10	Sequential 3D Registration	Detection+Tracking	2D Guided 3D registration	MultiView Median
Ours	74.39	92.57	2.14	0.99	81.10	Sequential 3D Registration	Detection+Tracking	2D Guided 3D registration	MultiView Mean
Ours	71.34	94.84	2.05	0.94	75.00	Sequential 3D Registration	Detection Peaks	Direct Index	Last Response
Ours	70.73	95.48	1.81	0.85	75.00	Sequential 3D Registration	Detection Peaks	Direct Index	MultiView Median
Ours	71.95	96.77	1.78	0.86	75.00	Sequential 3D Registration	Detection Peaks	Direct Index	MultiView Mean
Ours	76.22	94.94	2.06	0.96	80.49	Sequential 3D Registration	Detection Peaks	2D Guided 3D registration	Last Response
Ours	76.22	95.57	1.82	0.88	80.49	Sequential 3D Registration	Detection Peaks	2D Guided 3D registration	MultiviewMedian
Ours	77.44	96.84	1.78	0.89	80.49	Sequential 3D Registration	Detection Peaks	2D Guided 3D registration	MultiView Mean
Ours	70.73	97.18	1.47	0.66	73.17	Sequential 3D Registration	Groundtruth Track	Direct Index	Last Response
Ours	71.95	98.59	1.46	0.67	73.17	Sequential 3D Registration	Groundtruth Track	Direct Index	MultiView Median
Ours	71.95	98.59	1.47	0.67	73.17	Sequential 3D Registration	Groundtruth Track	Direct Index	MultiView Mean
Ours	76.83	97.32	1.45	0.65	79.27	Sequential 3D Registration	Groundtruth Track	2D Guided 3D registration	Last Response
Ours	78.05	98.66	1.43	0.67	79.27	Sequential 3D Registration	Groundtruth Track	2D Guided 3D registration	MultiviewMedian
Ours	78.05	98.66	1.44	0.67	79.27	Sequential 3D Registration	Groundtruth Track	2D Guided 3D registration	MultiView Mean

Table 4. **All Results on Validation Set.** In this table, we provide all possible results with our proposed methods for complete and exhaustive comparison.

VQ3D-Test	Succ%↑	Succ*%↑	L2↓	Angle↓	QwP%↑	(3.1) 3D Sparse Mapping & Camera Pose Estimation	(3.2) Video Object Detection from Visual Queries	(3.3) 3D pose Registration for Response Frames	(3.4) View Backprojection & Aggregation
Ego4D	8.71	51.47	4.93	1.23	15.15	Sim2Real	Detection + Tracking	Direct Index	Last Response
Ours	73.48	85.83	2.39	0.72	85.98	Sequential 3D Registration	Detection+Tracking	Direct Index	Last Response
Ours	75.76	87.85	2.32	0.70	85.98	Sequential 3D Registration	Detection+Tracking	Direct Index	MultiView Median
Ours	76.14	88.26	2.31	0.70	85.98	Sequential 3D Registration	Detection+Tracking	Direct Index	MultiView Mean
Ours	77.27	86.06	2.37	0.68	90.15	Sequential 3D Registration	Detection+Tracking	2D Guided 3D registration	Last Response
Ours	79.17	87.65	2.30	0.68	90.15	Sequential 3D Registration	Detection+Tracking	2D Guided 3D registration	MultiView Median
Ours	79.55	88.05	2.30	0.68	90.15	Sequential 3D Registration	Detection+Tracking	2D Guided 3D registration	MultiView Mean
Ours	77.65	90.35	2.22	0.68	87.12	Sequential 3D Registration	Detection Peaks	Direct Index	Last Response
Ours	80.68	92.66	2.04	0.64	87.12	Sequential 3D Registration	Detection Peaks	Direct Index	MultiView Median
Ours	83.33	95.75	1.95	0.62	87.12	Sequential 3D Registration	Detection Peaks	Direct Index	MultiView Mean
Ours	81.06	90.35	2.20	0.66	90.53	Sequential 3D Registration	Detection Peaks	2D Guided 3D registration	Last Response
Ours	84.09	92.66	2.03	0.62	90.53	Sequential 3D Registration	Detection Peaks	2D Guided 3D registration	MultiviewMedian
Ours	86.36	95.37	1.94	0.60	90.53	Sequential 3D Registration	Detection Peaks	2D Guided 3D registration	MultiView Mean

Table 5. All Results on Test Set. In this table, we provide all possible results with our proposed methods for complete and exhaustive comparison.

C. Hyperparameters

C.1. COLMAP

In this section, we provide the detailed hyperparameters we used for COLMAP [28].

C.1.1 Camera Intrinsic Estimation

We follow Ego4D [15] to estimate the camera intrinsic at first to save time for the sparse mapping later. We subsample 100 contiguous non-blurry frames from the videos selected by the variance of Laplacian, which will be fed into COLMAP auto reconstruction to estimate camera intrinsics. Then we will use the fixed camera intrinsics for all the videos.

C.1.2 Two Stage Registration

We use sequential_matcher at Stage 1 (Lst. 1) and vocab_matcher at Stage 2 (Lst. 2) for our sparse mapping and camera pose estimation, as mentioned in our main paper. Note that we omit some simple steps like feature extraction in Stage 1 as shown in Lst. 1. Note that we also perform local and global bundle adjustments in Stage 2 as shown in Lst. 2 after any successful image registration.

```
subprocess.run([
      'colmap', "sequential_matcher",
      "--database_path", "database.db",
      "-- Sequential Matching . vocab_tree_path",
      "vocab_tree_flickr100K_words256K.bin",
      "--SequentialMatching.loop_detection",
      "1",])
  subprocess.run([
      'colmap', "mapper", "--database_path", "
10
      database.db",
      "--Mapper.ba_global_max_num_iterations", "30"
      "--Mapper.ba_global_images_ratio", "1.4"])
```

Listing 1. Stage 1

```
subprocess.run([
       'colmap',
      "vocab_tree_matcher",
      "--database_path",
       "database.db",
      "--VocabTreeMatching.vocab_tree_path",
      "vocab\_tree\_flickr100\bar{K}\_words256K.bin"
      "--VocabTreeMatching.match_list_path",
      "unregistered_responses_list",
10 ])
  subprocess.run([
12
      'colmap',
      "image_registrator",
14
      "--database_path",
      "database.db",
16
      "--Mapper.init_min_num_inliers",
18
      "--Mapper.tri_ignore_two_view_tracks",
19
20
```

```
"--Mapper.abs_pose_min_num_inliers",
21
       "10"
22
23 ])
```

Listing 2. Stage 2

C.2. Video Object Detection

We follow the settings from Ego4D [15] VQ2D baseline for our detector and we remain all the hyperparameters of Siamese RCNN the same. We refer our readers to Ego4D Episodic Memory VQ2D Benchmark¹ for these settings.

D. Registration

The poses from COLMAP are independent of Matterport world coordinate system. We need to align our poses with the Matterport scan because volunteers make the ground truth annotations in those scans with respect to the Matterport scan coordinate system. We use the $model_aligner$ function provided by COLMAP to do the alignment between these two coordinate systems. We render at least three images from the Matterport scan with known camera poses. Then we use the script in Lst. 3 to estimate the Sim3 transform between our coordinate system reconstructed by COLMAP and Matterport Scan. In this way, we can evaluate our results in the same coordinate system where the volunteers annotate the ground truth 3D bboxes.

```
subprocess.run([
       'colmap', 'model_aligner',
      '--ref_images_path', 'matterport_renderings',
'--ref_is_gps', '0',
      '--robust_alignment', '1', '--alignment_type'
       , 'custom',
       '--estimate_scale', '1', '--
      robust_alignment_max_error', '25'
7 ])
```

Listing 3. Stage 2

 $^{^{1} \}verb|https://github.com/EGO4D/episodic-memory/tree/$ main/VO2D